

# Digital Twin for Autonomous Guided Vehicles based on Integrated Sensing and Communications

Van-Phuc Bui, Pedro Maia de Sant Ana, Soheil Gherekhloo, Shashi Raj Pandey, Petar Popovski

**Abstract**—This paper presents a Digital Twin (DT) framework for the remote control of an Autonomous Guided Vehicle (AGV) within a Network Control System (NCS). The AGV is monitored and controlled using Integrated Sensing and Communications (ISAC). In order to meet the real-time requirements, the DT computes the control signals and dynamically allocates resources for sensing and communication. A Reinforcement Learning (RL) algorithm is derived to learn and provide suitable actions while adjusting for the uncertainty in the AGV’s position. We present closed-form expressions for the achievable communication rate and the Cramer–Rao bound (CRB) to determine the required number of Orthogonal Frequency-Division Multiplexing (OFDM) subcarriers, meeting the needs of both sensing and communication. The proposed algorithm is validated through a millimeter-Wave (mmWave) simulation, demonstrating significant improvements in both control precision and communication efficiency.

## I. INTRODUCTION

Smart manufacturing in Industry 4.0 requires collection of extensive real-time data from a wide range of wireless sensors [1]. Unlike the traditional simulation tools or optimization techniques, digital twin (DT) models convert these large datasets into predictive models [2]. This enables simulation of various control strategies, thereby facilitating real-time interactions and decision-making for system operators [3].

A network control system (NCS) is used to power up a DT, where the latter can be situated either at the edge, tailored to local physical systems, or in the cloud, covering extensive physical systems. The network comprises sensor devices and/or central/distributed units integral to a 5G system or beyond [4]. The acquired knowledge from the DT model serves twofold purposes: (1) controlling the physical world; and (2) provision of monitoring system states. Traditionally, tracking the physical world relies upon wired/wireless connections for internal communications among sensors, controllers, and actuators. However, this can limit the agility and scalability of system because different sensors provide varying sensing accuracy and associated costs. Additionally, in a complex environment comprising multiple sensors and remote devices operating simultaneously, there is a significant burden on processing various types of signals and managing interference. To overcome these challenges, we advocate the use of Integrated Sensing and Communications (ISAC) [5], which leverages compact access points (APs) to enable simultaneous communication and monitoring physical world.

V.-P. Bui, S.R. Pandey, and P. Popovski (emails: {vpb, srp, petarp}@es.aau.dk) are all with the Department of Electronic Systems, Aalborg University, Denmark. P. M. de Sant Ana is with Corporate Research and Soheil Gherekhloo is with Cross-Domain Computing Solutions, both at Robert Bosch GmbH, Germany (email: {Pedro.MaiadeSantAna, soheil.gherekhloo}@de.bosch.com). This work was supported by the Villum Investigator Grant “WATER” from the Velux Foundation, Denmark.

There has been substantial research on ISAC covering foundational concepts, algorithms, analysis, and demonstrators [5], [6] [7]. It has been shown in [8] that the communication rate of ISAC systems can be maximized within radar performance constraints. DT frameworks are also applied in monitoring Automated Guided Vehicles (AGVs) by effectively selecting and scheduling UWB sensors for efficient demonstration in industry [9]. However, the aforementioned works [5]–[9] and their references do not consider the reciprocal influence between ISAC and control performance in the physical world based on communication requirements.

Here we examine the DT architecture for tracking dynamic changes in system parameters and efficiently controlling the AGV. We formulate an optimization problem to balance subcarrier allocation between sensing and communication, aiming to maintain the confidence of the DT’s system estimates while simultaneously optimizing the AGV control policy. We devise an RL agent that learns to perform actions while managing the uncertainty estimation of the state. A closed-form solution for subcarrier allocation is presented, tailored to meet the required AGV position uncertainty from both the RL agent and the DT. In terms of communication, we calculate the amount of subcarriers required to meet the throughput demand. We introduce an efficient solution to allocate the available subcarriers within a mmWave environment, balancing the needs of sensing and communication. The numerical results to validate our theoretical findings, offering a superior performance of the proposed subcarrier allocation scheme.

## II. DIGITAL TWIN ARCHITECTURE

### A. System model

We explore the application of ISAC to support NCSs within a DT framework for a AGV, as illustrated in Fig. 1. The DT model’s objective is to uphold a precise estimate of AGV’s state and offer optimized sequence of actions to be executed in the physical realm based on its beliefs about states. The AGV is monitored and controlled through set of APs deployed at the physical world. These APs synchronize their DTs, including locations and power budget status, with the Cloud platform with a high reliability and periodic synchronization overhead. Based on the current model state and the update from the AGV, the DT model updates the AGV’s active state, control policy, control signal, and schedules OFDM subcarriers for sensing and communication at the APs. The control problem considered here is known as the Mountain-Car Continuous problem [10], inspired by control systems for autonomously operating AGVs. The link between the AP and the cloud is assumed to be perfect. At the start of each query interval (QI),

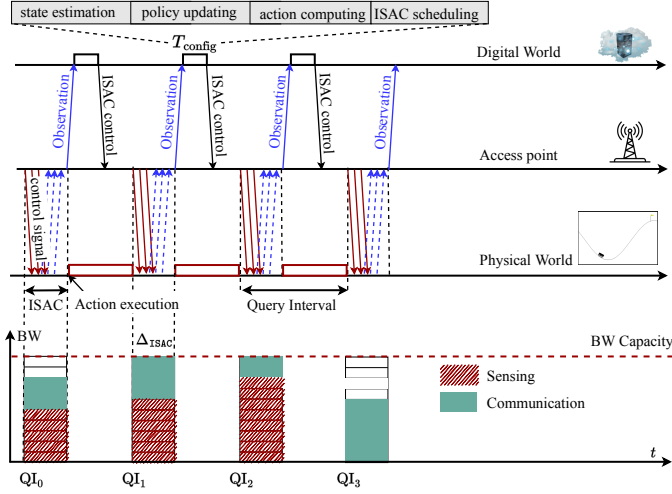


Fig. 1: The ISAC-based Digital Twin diagram.

the scheduled AP uses ISAC within  $\Delta_{\text{ISAC}}$  interval to sense the state and communicate with the AGV. The DT continuously monitors the AGV's state through APs and dynamically adjusts the control inputs to optimize its path. Our approach does not use no specific techniques for estimating the future state of the AGV, such that the control signals are calculated based on the previous state of the AGV. This is reasonable when the indoor AGV operates at a low speed and the QI length is short. The controller generates a command and sends it over a downlink channel. The application output for actuator control retrieves the latest commands from memory and applies them to the AGV. The AGV's state at any QI  $t$  is represented by  $\mathbf{s}_t = [x_t, v_t]$ , where  $x_t/v_t$  denotes the position/velocity, respectively, at QI  $t$ . The control signal  $a_t$  indicates the applied force. The system dynamics is modeled as

$$\mathbf{s}_{t+1} = f(\mathbf{s}_t) + \mathbf{B}a_t + \mathbf{u}_t, \forall t \in \mathcal{T}, \quad (1)$$

where  $f(\mathbf{s}_t) = \begin{bmatrix} x_t + v_t \\ v_t - \varphi \cos(3x_t) \end{bmatrix}$ ,  $\mathbf{B} = [0, \vartheta]^\top$ , with the constants  $\varphi = 0.0025$  and  $\vartheta = 0.0015$  [11].  $\mathbf{u}_t \sim \mathcal{N}(\mathbf{0}, \mathbf{C}_u)$  indicates the process noise.

### B. ISAC model

We consider a mono-static configuration featuring quasi co-located transmitters (TX) and receivers (RX) with equal characteristics, comprising  $R$  rows and  $C$  columns, and separated by distances  $\Delta r$  and  $\Delta c$ , respectively [12]. The budget at AP includes total  $N$  subcarriers and  $M$  OFDM symbols. The DT model attempts to schedule  $n_{s,t}$  subcarriers for sensing and  $n_{c,t} \leq N - n_{s,t}$  subcarriers for communication.

1) *Sensing model*: The received reflected signal  $r_t$  has the form  $r_t = b_t \varrho_{t-\tau_t} e^{j2\pi f_t^D t} e^{j\psi_t} + \tilde{z}_t$ , where the transmitted signal is  $\varrho_t$ , the delay  $\tau_t = 2r_t/c$ , the Doppler shift  $f_t^D = 2v_t/c$ , an addition random phase rotation  $\psi_t$ , and AWGN  $\tilde{z}_t \sim \mathcal{N}(0, \sigma_z^2)$ . The attenuation, using a point scatterer model, is  $b_t = \sqrt{\frac{c^2 \Psi}{(4\pi)^3 r_t^4 f_c^2}}$ . We denote by  $\Psi, r, \lambda, f_c, c$  the radar cross section, range, wavelength, central frequency, and speed of light, respectively. In LoS sensing, the received power  $P_t^{\text{R}} is:$

$$P_t^{\text{R}} = \frac{P^{\text{T}} G^{\text{T}}}{4\pi r_t^2} \Psi \frac{1}{4\pi r_t^2} \frac{G^{\text{R}} \lambda^2}{4\pi} = P^{\text{T}} G^{\text{T}} G^{\text{R}} b_t^2, \forall t \in \mathcal{T}, \quad (2)$$

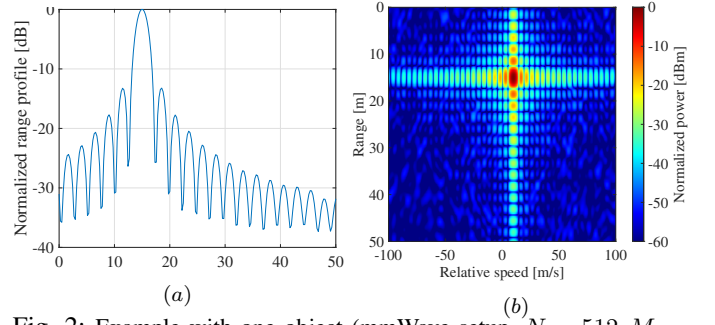


Fig. 2: Example with one object (mmWave setup,  $N = 512$ ,  $M = 128$ ): (a) Normalized range profile; and (b) a periodogram.

where  $P^{\text{T}}, G^{\text{T}}, G^{\text{R}}$  are transmitted power, transmit antenna array gain, receive antenna array gain, respectively, by assuming a perfect focus on the target with the transmit beam. The received noise power is  $P_t^{\text{N}} = (N_0 F)(n_{s,t} \Delta f)$ , where  $N_0$  is the noise spectral density,  $F$  is noise figure, and  $\Delta f$  the subcarrier spacing. The sensing Signal-to-Noise (SNR) ratio is calculated as [13]:

$$\gamma_{s,t} = \frac{P^{\text{R}} s}{P^{\text{N}}} n_{s,t} M = P^{\text{T}} G^{\text{T}} G^{\text{R}} \Psi \frac{c^2 M}{(4\pi)^3 r_t^4 f_c^2 N_0 F \Delta f}. \quad (3)$$

Assuming the transmitted OFDM frame is presented by  $\mathbf{F}^{\text{T}} \in \mathcal{F}^{N \times M}$  where  $\mathcal{F}$  is the modulation alphabet. Specially, each row of  $\mathbf{F}^{\text{T}}$  represents a sub-carrier; each column represents an OFDM symbol of the transmitted frame. Then the element  $(n, m)$  of the received frame matrix  $\mathbf{F}_t^{\text{R}}$  at intervals of length  $T_0$  is computed by  $[\mathbf{F}_t^{\text{R}}]_{(n,m)} = b e^{j2\pi m T_0 f_t^D} e^{-j2\pi n \tau_t \Delta f} e^{j\psi_t} + [\mathbf{Z}_t]_{(n,m)}$ . Using solution from [14], the periodogram of  $\mathbf{F}_t^{\text{R}}$  is formulated as

$$[\text{Per}_t^{\text{F}}]_{(n,m)} = \frac{\left| \sum_{k=0}^{N_{\text{Per}}-1} \left( \sum_{l=0}^{M_{\text{Per}}-1} [\mathbf{F}_t]_{(k,l)} e^{-j2\pi \frac{lm}{M_{\text{Per}}}} \right) e^{j2\pi \frac{kn}{N_{\text{Per}}}} \right|^2}{NM}.$$

AGV's estimated range and velocity are computed by  $\hat{r}_t = (\text{Pe}_t^{\hat{r}} c) / (2\Delta f N_{\text{Per}})$  and  $\hat{v} = (\text{Pe}_t^{\hat{v}} c) / (2f_c T_0 M_{\text{Per}})$ . Herein,  $\text{Pe}_t^{\hat{r}}$  and  $\text{Pe}_t^{\hat{v}}$  are respectively peak values of the matrix  $\text{Per}_t^{\text{F}}$ .  $N_{\text{Per}}$  and  $M_{\text{Per}}$  are the number of IFFT and FFT in transformation, respectively. Fig. 2 plots the normalized range profile and an example of a periodogram to sense the range and speed under mmWave setup. The Cramér-Rao Bound (CRB) establishes a minimum limit on the variance of unbiased estimators. Within the considered framework, we outline the uncertainty for position and velocity, specifically for the purposes of monitoring and estimating within the DT model. To achieve this, we first derive the CRB for estimating the target's range, velocity, and elevation angle as [5]

$$\sigma_{r,t} = \frac{c}{4\pi \Delta f} \sqrt{\frac{6}{(n_{s,t}^2 - 1) \gamma_t^{\text{R}}}}, \forall t \in \mathcal{T}, \quad (4)$$

$$\sigma_{v,t} = \frac{c}{4\pi f_c T_0} \sqrt{\frac{6}{(M^2 - 1) \gamma_t^{\text{R}}}}, \forall t \in \mathcal{T}, \quad (5)$$

$$\sigma_{\theta,t} = \sin^{-1} \left( \frac{\lambda}{\Delta c} \cos(\phi_t) (\ell_t \pm \sigma_{\text{fx},t}) \right) - \theta_t, \forall t \in \mathcal{T}, \quad (6)$$

where  $\sigma_{\text{fx},t}^2 = 6 / ((R^2 - 1) 4\pi^2 \gamma_t)$  is the normalized angular frequencies (NAFs) in horizontal direction of the receive array [15]. The NAF  $\ell_t$  is calculated by  $\ell_t = (\Delta c \sin(\theta_t)) / (\lambda \cos(\phi_t))$ . Note that  $\sigma_{v,t}$  does not depend on

the number of allocated subcarriers and we focus on the effect of AGV's position uncertainty to calculate the control signal.

2) *Communication Model*: With multiple TX antennas, the received signal at AGV from transmitted waveform  $\omega_t \in \mathbb{C}^{RC}$  is  $y_t = \mathbf{h}_t^H \omega_t + w_t$ , where  $w_t \sim \mathcal{N}(0, \sigma_{w,t}^2)$  is the AWGN with  $\sigma_{w,t}^2 = (N_0 F)(n_{c,t} \Delta f)$ . The frequency flat fading channel between AP and the user is  $\mathbf{h}_t = \beta_t^{1/2} \bar{\mathbf{h}}_t \in \mathbb{C}^{RC}$ , where  $\beta_t = \frac{n_{c,t} G^T c^2}{(4\pi r_t f_c)^2}$  is the large-scale fading and  $\bar{\mathbf{h}}_t$  the small-scale fading. We assume it is independent between communication and sensing process, leading to the channel is first estimated via uplink training, which is then used for the downlink transmission. Let  $\tau_p^c$  and  $\tau_{\text{tot}}^c$  be the length of the pilot sequences and coherence interval in samples, respectively, with  $\tau_p^c < \tau_{\text{tot}}^c$ . When AGV send their pilot sequence  $\sqrt{\tau_p^c} \boldsymbol{\varpi} \in \mathbb{C}^{\tau_p^c}$ , the received pilot signal at the AP is given by  $\mathbf{Y}_t = \sqrt{\tau_p^c} p_p \mathbf{h}_t \boldsymbol{\varpi}^H + \mathbf{N}_{p,t}$ , where  $\mathbf{N}_{p,t} \in \mathbb{C}^{RC \times \tau_p^c}$  is the AP noise, whose entries are independent and identically distributed (i.i.d.)  $\mathcal{N}(0, \sigma^2)$ , and  $p_p$  is the average power of the training symbols. To estimate  $\mathbf{h}_t$ , we project  $\mathbf{Y}_t$  onto  $\boldsymbol{\varpi}$  as  $\mathbf{y}_t = \mathbf{Y}_t \boldsymbol{\varpi} = \sqrt{\tau_p^c} p_p \mathbf{h}_t + \mathbf{n}_{p,t}$ , where  $\mathbf{n}_{p,t} = \mathbf{N}_{p,t} \boldsymbol{\varpi}$  is additive noise at the AP section, which is Gaussian  $\mathbf{n}_{p,t} \sim \mathcal{N}(\mathbf{0}, \sigma_p^2 \mathbf{I}_{RC})$ . As a result, the MMSE channel estimate is  $\hat{\mathbf{h}}_t = (\sqrt{\tau_p^c} p_p \beta_t \mathbf{Y}_t \boldsymbol{\varpi}) / (\tau_p^c p_p \beta_t + \sigma_p^2)$ . In another word,  $\hat{\mathbf{h}}_t$  follows  $\hat{\mathbf{h}}_t \sim \mathcal{N}(\mathbf{0}, \sigma_{\hat{h},t}^2 \mathbf{I}_{RC})$ , where  $\sigma_{\hat{h},t}^2 = \tau_p^c p_p \beta_t^2 / (\tau_p^c p_p \beta_t + \sigma_p^2)$ . It is noted that the channel estimation error  $\mathbf{e}_t = \mathbf{h}_t - \hat{\mathbf{h}}_t$  follows  $\mathbf{e}_t \sim \mathcal{N}(\mathbf{0}, \epsilon_t^2 \mathbf{I}_{RC})$  whose  $\epsilon_t^2 = \beta_t - \sigma_{\hat{h},t}^2$ . The achievable SNR at the AGV is  $\gamma_{c,t} = (P^T \sigma_{\hat{h},t}^2) / (P^T \epsilon_t^2 + \sigma_{w,t}^2)$ . We approximate the achievable communication rate by  $R_t(n_{c,t}) = \bar{\tau}_t n_{c,t} \Delta f \log_2(1 + \gamma_{c,t})$  with  $\bar{\tau}_t = (\tau_{\text{tot},t} - \tau_{p,t}) / \tau_{\text{tot},t}$ .

### C. Problem Formulation

Our goal is to maintain optimal control signals by implementing a control policy that meets the AGV's maximum allowable position variance and optimizes resource allocation for sensing and communication. The maximal acceptable variance for AGV's position is defined as

$$\sigma_{x,t}^2 \leq \xi^2, \forall t \in \mathcal{T}. \quad (7)$$

$V^\pi(\hat{\mathbf{s}}_0)$  is defined as the value function of controlling AGV in (1) under the control policy  $\pi$ , which is detailed in the next section. Our primary objective is to jointly minimize the total power consumption while ensuring the delivery of optimal control signals. Here  $h(\{n_{s,t}\}, \{n_{c,t}\}, \{a_t\}) = \left[ V^\pi(\hat{\mathbf{s}}_0), -\sum_{t=0}^{\infty} (n_{s,t} + n_{c,t}) \right]^T$ , is a multi-objective function, encompassing the two performance metrics. We formulate the optimization problem as a joint design of control and scheduling  $\{n_{s,t}, n_{c,t}\}$  while maintaining the confidence of DT's system estimate as follows

$$\underset{\{n_{s,t}\}, \{n_{c,t}\}, \{a_t\}}{\text{maximize}} \quad h(\{n_{s,t}\}, \{n_{c,t}\}, \{a_t\}) \quad (8a)$$

$$\text{s.t.} \quad \mathbf{s}_t = f(\mathbf{s}_{t-1}) + \mathbf{B}a_{t-1} + \mathbf{u}_t, \quad (8b)$$

$$R_t(n_{c,t}) \geq \bar{R}, \forall t \in \mathcal{T}, \quad (8c)$$

$$\sigma_{x,t}^2 \leq \xi^2, \forall t \in \mathcal{T}, \quad (8d)$$

$$n_{s,t} + n_{c,t} \leq N, \forall t \in \mathcal{T}. \quad (8e)$$

In order to maintain the communication Quality-of-Service (QoS) at every QI  $t$ , the throughput threshold  $\bar{R}$  in (8b) is employed. The constraint (8e) ensures that the total number of subcarriers used  $n_{s,t} + n_{c,t}$  does not exceed the system capacity  $N$ . It is noted that we examine a context in which the belief vector is controlled via ISAC supported by DT before being employed by RL to propose the optimal action as an outcome, thereby allowing the agent to make precise decisions.

In the following, we introduce proposed a heuristic solution, which incorporates a two-step approach to effectively address (8): (i) an uncertainty control RL algorithm is utilized to devise control actions for the physical world, effectively managing state estimation errors; (ii) Subcarrier optimization algorithm is applied to identify suitable  $\{n_{s,t}, n_{c,t}\}$ , guided by the requirements of the RL model and DT.

### III. UNCERTAINTY CONTROL POMDP

The control problem in (8) is treated as a Partially Observable Markov Decision Process (POMDP), an extension of the Markov Decision Process (MDP) that includes sets of observations and observation probabilities due to partial and potentially inaccurate information. In particular, the agent maintains an estimate vector  $\hat{\mathbf{s}}_t$ , which describes the probability of being in a state  $\mathbf{s}_t$ . The policy  $\pi(\hat{\mathbf{s}}, \mathbf{a})$  of the agent specifies an action  $\mathbf{a}_t$  based on this estimate, represented as  $\pi(\hat{\mathbf{s}}, \mathbf{a})$ . Given an initial belief  $\hat{\mathbf{s}}_0$ , the expected future discounted reward for the policy  $\pi(\hat{\mathbf{s}}, \mathbf{a})$  is expressed as  $V^\pi(\hat{\mathbf{s}}_0) = \mathbb{E}[\sum_{t=0}^{\infty} \gamma_t r(\mathbf{s}_t, \mathbf{a}_t, \mathbf{s}_{t+1}) \mid \hat{\mathbf{s}}_0, \pi]$ , where  $0 < \gamma_t < 1$  is the discount factor. At QI  $t$ , the estimated state vector is  $\hat{\mathbf{s}}_t = [\hat{x}_t, \hat{v}_t]^T \in \mathbb{R}^2$ , governed by the conditional probability distribution function  $\hat{\mathbf{s}}_t \sim p(\hat{\mathbf{s}}_t \mid \mathbf{s}_t; \eta_t)$ , where  $\eta_t \in \mathbb{R}^1$  is parameterized by the accuracy of AGV's position. We define  $\eta_t = 1/\sigma_{x,t}^2$ . As  $\eta_t$  increases, the confidence in  $\hat{x}_t$  improves, enabling the RL agent to make more accurate decisions. However, achieving high reliability for  $\hat{x}_t$  requires low measurement error, which increases corresponding  $n_{s,t}$  and processing costs. For training  $\pi(\hat{\mathbf{s}}, \mathbf{a})$ , we employ Proximal Policy Optimization (PPO) with the actor-critic structure at RL agents that involves dividing the model into two distinct components, thus harnessing the strengths of both value-based and policy-based methods [16]. To tackle the joint design problem aimed at optimizing actions while minimizing communication energy, we employ the Deep RL approach within the DT cloud environment, where the action and reward are defined as follows.

1) *Action Space Reformulation*: The action vector in the RL agent, structured as  $\mathbf{a}_t = [a_t, \eta_t]$ , comprises control signals  $a_t$  that affect the environment and  $\eta_t$  for accuracy in estimated position. This study addresses optimizing the RL agent's state estimation accuracy, allowing continuous selection of  $\eta_t$ . The framework aims to reveal the informational value of observations for the task.

2) *Reward Function Reformulation*: It is essential for the RL agent to not only pursue the primary goal defined by the problem but also to develop the capability to control the acceptable accuracy level  $\eta_t$ . The goal-oriented reward  $r_t$  is adjusted into an uncertainty-based reward  $\tilde{r}_t = r_t + \kappa \eta_t$ , where  $\kappa \geq 0$  serves as a weighting factor. The agent's dual objective

---

**Algorithm 1** Proposed solution to the problem (8)

---

**Input:** System capacity  $N$ , DT requirement  $(\xi_t, \bar{R})$ 
**Output:**  $(n_{c,t}, n_{s,t})$ ,  $R_{c,t}$ , and  $\hat{s}_t$ 
*Control strategy:*

1: Choose optimal action  $\mathbf{a}_t$  in estimated state  $\hat{\mathbf{s}}_t$  according to trained policy  $\pi^*$ 
*Subcarrier allocation for ISAC strategy:*

2: Compute required  $n_{s,t}$  as in (12)

3: Compute required  $n_{c,t}$  as in (10)

4: **if**  $n_{c,t} > N$  **then**

5:      $n_{c,t}^* = N, n_{s,t}^* = 0$ 

6: **else if**  $n_{c,t} < N$  and  $n_{c,t} < N + n_{s,t} > N$  **then**

7:      $n_{c,t}^* = n_{c,t}, n_{s,t}^* = N - n_{c,t}^*$ 

8: **else**

9:      $n_{c,t}^* = n_{c,t}, n_{s,t}^* = n_{s,t}$ 

10: **end if**

11: Update  $\hat{s}_t$ 

12: Update throughput  $R_{c,t}$ 


---

is to maximize the original reward while concurrently minimizing the cost associated with observations.

#### IV. SUBCARRIER OPTIMIZATION FOR DT

The subcarrier allocation for communication and sensing will be based on: (i) the acceptable level of accuracy  $\eta_t$  for the estimated state, as determined by the RL agent; (ii) the accuracy requirements of the DT model as specified in (7); and (iii) the availability of wireless resources, determined by the system capacity and data rate requirements (2).

1) *Reformulation Problem* : We introduce arbitrary variables  $\bar{\xi}_t^2$  indicates desired DT's error level of system's state at QI  $t$ . Given the reliability for the DT in (7) and the requisite level of accuracy  $\eta_t$  to uphold the precision of the RL model, the DT should meet the error constraints at QI  $t$  as  $\sigma_{x,t}^2 \leq \bar{\xi}_t^2 \triangleq \min\left\{\xi^2, \frac{1}{\eta_t}\right\}$ . At the QI  $(t-1)$  we solve the optimization problem

$$\text{P1: minimize}_{n_{s,t}, n_{c,t}} \alpha_1 \max\{\sigma_{x,t}^2 - \bar{\xi}_t^2, 0\} + \alpha_2(n_{s,t} + n_{c,t}) + \alpha_3|R_t(n_{s,t}) - \bar{R}, 0| \quad (9a)$$

$$\text{s.t. } n_{s,t} + n_{c,t} \leq N, \quad (9b)$$

wherein the non-negative parameter  $\alpha_1, \alpha_2, \alpha_3 \in [0, 1]$  represents the relative weight to accuracy and energy efficiency within the underlying objective function. The objective (9a) relaxes the constraints (8c) and (8d) due to its dependence on practical conditions, i.e., in situations where the error surpasses a certain threshold, even utilizing all subcarrier capacity fails to guarantee the desired reliability  $\bar{\xi}_t^2$ .

2) *Communication subcarrier allocation*: The required  $n_{c,t}^*$  to satisfied the communication constraint  $R_t(n_{c,t}) \geq \bar{R}$  is obtained in closed-form by definition as

$$n_{c,t}^* \geq \frac{\bar{R}}{\bar{r}_t \Delta f \log_2(1 + \gamma_{c,t})}, \forall t \in \mathcal{T}. \quad (10)$$

3) *Sensing subcarrier allocation*: We emphasize that the target position uncertainty can be calculated in closed form based on the range (4) and angle (6) uncertainties, as established by the following lemma.

**TABLE I: Simulation Parameters**

Parameter	Value	Parameter	Value
Carrier frequency ( $f_c$ )	28 GHz	Subcarrier spacing ( $\Delta f$ )	120 kHz
Bandwidth ( $B$ )	1600 MHz	Symbol duration ( $T_0$ )	8.92 $\mu$ s
Number of subcarriers ( $N$ )	512	Number of symbols ( $M$ )	128
Noise figure ( $F$ )	8 dB	Transmit antenna gain ( $G_T$ )	33 dB
Receive antenna gain ( $G_E$ )	3 dBi	Transmit power ( $P_T$ )	25 dBm
The reward weight ( $\kappa$ )	$5 \times 10^{-6}$	Antenna spacing ( $\Delta r, \Delta c$ )	0.5 $\lambda, 0.5\lambda$
Data rate threshold $\bar{R}$	1000 [Mbps]	$(N_{\text{Per}}, M_{\text{Per}})$	(6400, 5120)

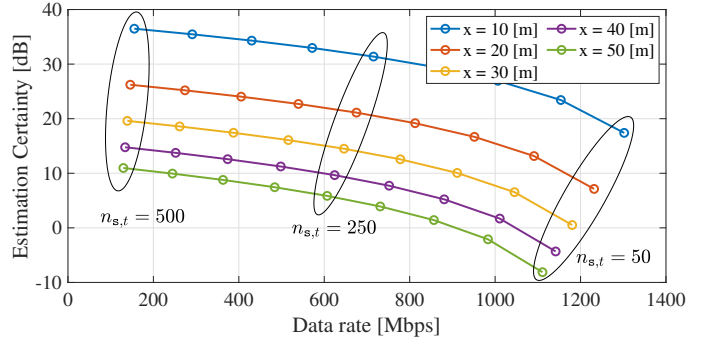


Fig. 3: Trade-off analysis between sensing certainty and communication data rate at various distances.

**Lemma 1.** From the distributions of range and elevation angle, specified as  $r_t$  with mean  $\bar{r}_t$  and variance  $\sigma_{r,t}^2$ , and  $\theta_t \sim \mathcal{N}(\bar{\theta}_t, \sigma_{\theta,t}^2)$  respectively, the position of the AGV  $x_t$ , with its mean  $\bar{x}_t$  and variance  $\sigma_{x,t}^2$  follows

$$\begin{cases} \bar{x}_t = \bar{r}_t \cos(\bar{\theta}_t) e^{-\sigma_{\theta,t}^2/2}, \\ \sigma_{x,t}^2 = \Gamma_t + \sigma_{r,t}^2 \Upsilon_t, \end{cases} \quad (11)$$

where  $\Gamma_t = \bar{r}_t^2 \left( \frac{1}{2} + \frac{1}{2} \cos(2\bar{\theta}_t) e^{-2\sigma_{\theta,t}^2} - \left( \cos(\bar{\theta}_t) e^{-\sigma_{\theta,t}^2/2} \right)^2 \right)$ ,  $\Upsilon_t = \frac{1}{2} + \frac{1}{2} \cos(2\bar{\theta}_t) e^{-2\sigma_{\theta,t}^2}$ .

*Proof.* Please see the Appendix A.  $\square$

The mean value and variance of the AGV position are obtained from Lemma 1. With  $\sigma_{x,t}^2 \leq \delta^2$ , the sensing constraint can be formulated by  $\Gamma_t + \sigma_{r,t}^2 \Upsilon_t \leq \bar{\xi}_t^2$ , leading to the closed-form lower bound of  $n_{s,t}$  as

$$n_{s,t} \geq \sqrt{\frac{6c^2 \Upsilon_t}{(\bar{\xi}_t^2 - \Gamma_t)(4\pi \Delta f)^2 \gamma_{s,t}}} + 1, \quad (12)$$

which can solveable by selecting the optimal  $n_{s,t}$  that satisfying both (12) and the subcarrier capacity  $N$ . The proposed algorithm for solving (8) is outlined in Alg. 1.

#### V. SIMULATION RESULTS

In this section, we provide the numerical results to investigate our findings and proposed design. The important parameters are listed in Table I. Unless otherwise noted, at each QI, the AGV is served by the nearest AP with a distance randomly ranging from 5 to 30 meters, and the DT requirement  $\delta_t = 0.02 \forall t$ . In Fig. 3, we plot the trade-off between sensing certainty,  $1/\sigma_x^2$ , and achievable data rate,  $R_{c,t}$ , for different positions of the AGV. The number of subcarrier for communication with each value of  $n_{s,t}$  is  $n_{c,t} = N - n_{s,t}$ . It is evident that as more communication resources are allocated to sensing, the accuracy of the estimated position improves, while the AGV's throughput correspondingly decreases. Specifically, for

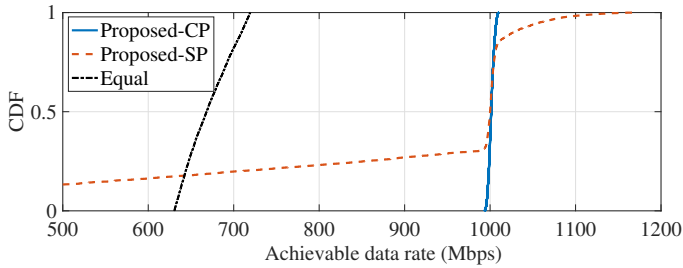


Fig. 4: The achievable data rate of different schemes.

a typical distance of 20m, if the AP allocates 250 subcarriers to sensing, the position estimation certainty is 7.5 dB, and the corresponding data rate is 600 Mbps. Decreasing  $n_{s,t}$  to 50 results in an AGV throughput of approximately 1100 Mbps, while the position uncertainty of the estimate is -9 dB. Recognizing this trade-off is crucial for optimizing the system in various applications with differing sensing and communication requirements.

The CDF of the achievable data rate among different algorithms is presented in Fig. 4 and their corresponding number of QI to reach the target in Fig. 5. In these figure, *Proposed-CP* (Proposed Communication Priority), depicted in Alg. 1, prioritizes allocating  $n_{c,t}$  to meet  $\bar{R}$  before allocating for  $n_{s,t}$ . *Proposed-SP* (Proposed Sensing Priority), also follows Alg. 1 but prioritizing subcarriers for sensing the AGV's position before allocating them for communication. The *Equal* method allocates subcarriers equally for sensing and communication as  $N/2$  at all times. Compared to the baseline, our schemes demonstrate superior performance in serving the AGV communication needs. It is noted that although the Proposed-CP achieves better communication performance, with  $R_{c,t}$  meeting  $\bar{R}$  most of the time compared to *Proposed-SP*, which fails to meet  $\bar{R}$  nearly 30% of the time, the AGV takes longer to reach the target due to sensing requirements not meeting the RL request as in Fig. 5.

## VI. CONCLUSIONS

This paper analyzes the impact of ISAC design within a DT framework for optimal system monitoring and control. By calculating the number of subcarriers required for sensing object positions and meeting communication requirements, we can easily propose options for efficient and economical wireless resource allocation. Our future work aims to extend the DT using ISAC in complex and practical environments with multiple AGVs moving and computing in indoor settings.

### APPENDIX A

Lets  $x_t$  follows a distribution with mean value as  $\bar{x}_t$  and variance  $\sigma_{x,t}^2$ . To find  $\bar{x}_t$ , we do have

$$\bar{x}_t = \mathbb{E}[r_t \cos(\theta_t)] = \mathbb{E}[r_t] \mathbb{E}[\cos(\theta_t)] = R_0 \cos(\bar{\theta}_t) e^{-\sigma_{\theta,t}^2/2}.$$

Next, to compute the variance  $\sigma_{x,t}^2$ , we have the fact that

$$\begin{aligned} \sigma_{x,t}^2 &= \mathbb{E}[r_t^2] \text{Var}[\cos(\theta_t)] + \text{Var}[r_t] \mathbb{E}[\cos^2(\theta_t)] \\ &= \bar{r}_t^2 \text{Var}[\cos(\theta_t)] + \sigma_{r,t}^2 \mathbb{E}[\cos^2(\theta_t)]. \end{aligned} \quad (13)$$

In (13), the goal is to convert  $\mathbb{E}[\cos^2(\theta_t)]$  and  $\text{Var}[\cos(\theta_t)]$  to tractable forms. First,  $\mathbb{E}[\cos^2(\theta_t)]$  can be equivalently

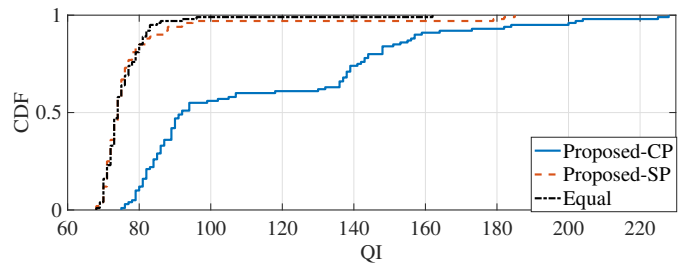


Fig. 5: Number of QI for AGV to reach the target.

reformulated as  $\mathbb{E}[\cos^2(\theta_t)] = \mathbb{E}[0.5(1 + \cos(2\theta_t))] = 0.5 + 0.5\mathbb{E}[\cos(2\theta_t)] = 0.5 + 0.5 \cos(2\bar{\theta}_t) e^{-2\sigma_{\theta,t}^2}$ . Using this result, we can rewrite  $\text{Var}[\cos(\theta_t)]$  to tractable manner as  $\text{Var}[\cos(\theta)] = \mathbb{E}[\cos^2(\theta)] - (\mathbb{E}[\cos(\theta)])^2 = \frac{1}{2} + \frac{1}{2} \cos(2\theta_0) e^{-2\sigma_{\theta}^2} - (\cos(\theta_0) e^{-\sigma_{\theta}^2/2})^2$ . Summing up, the  $\sigma_{x,t}^2$  is given by

$$\begin{aligned} \sigma_{x,t}^2 &= \bar{r}_t^2 \left( \frac{1}{2} + \frac{1}{2} \cos(2\bar{\theta}_t) e^{-2\sigma_{\theta,t}^2} - (\cos(\bar{\theta}_t) e^{-\sigma_{\theta,t}^2/2})^2 \right) \\ &\quad + \sigma_{r,t}^2 \left( \frac{1}{2} + \frac{1}{2} \cos(2\bar{\theta}_t) e^{-2\sigma_{\theta,t}^2} \right). \end{aligned} \quad (14)$$

By denoting  $\Gamma_t$  and  $\Upsilon_t$  as in (11), we obtain  $\sigma_{x,t}^2$  as in (11) and complete the proof.

## REFERENCES

- [1] Y. Tang *et al.*, "Tracking control of networked multi-agent systems under new characterizations of impulses and its applications in robotic systems," *IEEE Trans. Ind. Electron.*, vol. 63, no. 2, pp. 1299–1307, 2015.
- [2] Z. Wei *et al.*, "Integrated sensing and communication driven digital twin for intelligent machine network," *IEEE Internet Things Mag.*, vol. 7, no. 4, pp. 60–67, 2024.
- [3] S. Mihai *et al.*, "Digital twins: A survey on enabling technologies, challenges, trends and future prospects," *IEEE Commun. Surveys Tut.*, vol. 24, no. 4, pp. 2255–2291, 2022.
- [4] E. Dahlman, S. Parkvall, and J. Skold, *5G NR: The next generation wireless access technology*. Academic Press, 2020.
- [5] S. Mandelli *et al.*, "Survey on integrated sensing and communication performance modeling and use cases feasibility," in *Proc. IEEE 6GNet*, 2023, pp. 1–8.
- [6] A. Liu *et al.*, "A survey on fundamental limits of integrated sensing and communication," *IEEE Commun. Surv. Tutor.*, vol. 24, no. 2, pp. 994–1034, 2022.
- [7] "HEXA-X-II project," <https://hexa-x-ii.eu/>, 2024, accessed: 2024-07-25.
- [8] N. T. Nguyen, N. Shlezinger, Y. C. Eldar, and M. Juntti, "Multiuser mimo wideband joint communications and sensing system with subcarrier allocation," *IEEE Trans. Signal Process.*, 2023.
- [9] V.-P. Bui, D. Abode, P. M. Ana, K. Muthineni, S. R. Pandey, and P. Popovski, "Digital twin of industrial networked control system based on value of information," *arXiv preprint arXiv:2404.14960*, 2024.
- [10] A. W. Moore, "Efficient memory-based learning for robot control," University of Cambridge, Computer Laboratory, Tech. Rep., 1990.
- [11] "Gymnasium classic control: Mountain car continuous environment," [https://gymnasium.farama.org/environments/classic\\_control/mountain\\_car\\_continuous/](https://gymnasium.farama.org/environments/classic_control/mountain_car_continuous/), 2024, accessed: 2024-08-05.
- [12] T. Wild, A. Grudnitsky, S. Mandelli, M. Henninger, J. Guan, and F. Schaich, "6G Integrated Sensing and Communication: From Vision to Realization," *arXiv 2305.01978*, 2023. [Online]. Available: <https://arxiv.org/abs/2305.01978>
- [13] K. M. Braun, "OFDM radar algorithms in mobile communication networks," Ph.D. dissertation, Karlsruhe, Karlsruher Institut für Technologie (KIT), Diss., 2014, 2014.
- [14] C. Sturm and W. Wiesbeck, "Waveform design and signal processing aspects for fusion of wireless communications and radar sensing," *Proc. IEEE*, vol. 99, no. 7, pp. 1236–1259, 2011.
- [15] S. Mandelli, M. Henninger, and J. Du, "Sampling and reconstructing angular domains with uniform arrays," *IEEE Trans. Wireless Commun.*, vol. 22, no. 6, pp. 3628–3642, 2022.
- [16] V. Konda and J. Tsitsiklis, "Actor-critic algorithms," *Proc. NIPS*, vol. 12, 1999.